

Resonant absorption in complicated plasma configurations: applications to multi-stranded coronal loop oscillations

J. Terradas, I. Arregui, R. Oliver, J. L. Ballester

Departament de Física, Universitat de les Illes Balears, E-07122 Palma de Mallorca, Spain

and

J. Andries, M. Goossens

*Centre for Plasma Astrophysics, Katholieke Universiteit Leuven, Celestijnenlaan 200B,
B-3001 Leuven, Belgium*

jaume.terradas@uib.es

ABSTRACT

We study the excitation and damping of transverse oscillations in a multi-stranded model of a straight line-tied coronal loop. The transverse geometry of our equilibrium configuration is quite irregular and more realistic than the usual cylindrical loop model. By numerically solving the time-dependent ideal magnetohydrodynamic equations in two dimensions we show how the global motion of the whole bundle of strands, excited by an external disturbance, is converted into localized Alfvénic motions due to the process of resonant absorption. This process produces the attenuation of the transverse oscillations. At any location in the structure two dominant frequencies are found, the frequency of the global mode, or quasi-mode, and the local Alfvén frequency. We find that the mechanism of mode conversion, due to the coupling between fast and Alfvén waves, is not compromised by the complicated geometry of the model. We also show that it is possible to have energy conversion not only at the external edge of the composite loop but also inside the structure. The implications of these results and their relationship with the observations are discussed.

Subject headings: MHD — Sun: corona — Sun: magnetic fields — waves

1. Introduction

The resonant coupling of fast magnetohydrodynamic (MHD) waves and Alfvén waves has been an active research topic for many years. The most important applications are to

laboratory plasmas, the solar corona, and pulsations in the Earth’s magnetosphere. In the present paper we concentrate on the application of resonant absorption as a possible candidate to explain the damping of transverse coronal loop oscillations (see Hollweg & Yang 1988; Goossens et al. 1992; Ruderman & Roberts 2002; Terradas et al. 2006a). The attenuation of the loop oscillations, interpreted as the kink modes, is due to the energy conversion from the global large scale motions to localized Alfvén modes.

The time-dependent resonant absorption mechanism has been traditionally analyzed for both driven and initial value problems using different equilibrium models. For the driven problem this mechanism has been studied in smooth transition layers (Hollweg 1987; Davila 1987; Hollweg & Yang 1988), in slab models (Steinolfson & Davila 1993; Ofman et al. 1994; Ofman & Davila 1995; Ofman et al. 1995; De Groof & Goossens 2000, 2002), and in cylindrical tubes (Grossmann & Smith 1988; Poedts et al. 1989, 1990; Poedts & Kerner 1991; Sakurai et al. 1991; Goossens et al. 1995). For the initial value problem similar studies have also focused on smooth interfaces (Ionson 1978; Lee & Roberts 1986), on slabs (Steinolfson & Davila 1993), and cylinders (Ruderman & Roberts 2002; Terradas et al. 2006a). The effects of background flows have been investigated by Hollweg et al. (1990); Erdéyi & Goossens (1996); Tirry et al. (1998); Andries et al. (2000); Andries & Goossens (2001).

The time-dependent results have been complemented by eigenmode calculations (see for example Tirry & Goossens 1996). The coupling of the fast kink mode with the Alfvén continuum produces the damping of the oscillations. In this case the global mode is usually called the quasi-mode and has a complex frequency. The theoretical models that have been used to calculate the quasi-modes are so far simple but necessary to understand the main properties of resonant absorption. Recently, new effects have been investigated. The curvature effect has been studied by Van Doorselaere et al. (2004b) and Terradas et al. (2006b), and the influence of stratification along the loop has been analyzed by Andries et al. (2005) and by Arregui et al. (2005). The effect of non-circularity of the tube cross-section has been analyzed by Ruderman (2003), while the effect of the internal structure in loops, using a slab model, has been studied by Arregui et al. (2007). The overall conclusion of these recent investigations is that these new ingredients do not significantly change the damping per period of the oscillations. This suggests that resonant absorption is a robust mechanism and that its efficiency is not easily affected by the considered effects.

Nevertheless, even the most recent models are still too simple compared with the real conditions in coronal loops. For example, there are no physical reasons to think that the cross-section of coronal loops is perfectly cylindrical. Moreover, there is observational information suggesting that loops are not monolithic (as they are usually modeled) but that they are formed by bundles of individual strands considered as mini-loops for which the heating

and plasma properties are approximately uniform in the transverse direction (Schmelz et al. 2005). This view is supported by some authors (Martens et al. 2002; Klimchuk 2006) but not by others (Aschwanden 2005; Aschwanden & Nightingale 2005). Thus, one of the questions that arise from these observations is how the internal structure of coronal loops can modify the mechanism of resonant absorption.

The purpose of this paper is to study the mechanism of resonant absorption and its efficiency in a rather arbitrary two-dimensional distribution of plasma, and to analyze the implications on the damping of transversal coronal loop oscillations in a multi-stranded loop model. Instead of calculating the eigenmodes of the structure, which is difficult due to the complicated geometry, we investigate the dynamical response of the bundle of individual strands to an initial perturbation. Thus, we study the initial value problem of the excitation of the composite loop by solving the time-dependent two-dimensional ideal MHD equations. The equations are solved numerically using an appropriate code. From the simulations we study the motions in the loop structure and analyze how the energy from the global mode is converted into localized Alfvénic motions in the inhomogeneous regions of the loop.

This paper is organized as follows. In § 2 the multi-stranded loop model is described and the basic MHD equations are given. The numerical method used to solve the time-dependent equations is explained in § 3. In § 4 the results of the time-dependent problem for a single cylindrical inhomogeneous loop are compared with the eigenmode calculations. In § 5 the time-dependent problem for the multi-stranded loop is considered and several features of the resonant absorption mechanism are discussed, in particular the behavior in the inhomogeneous layer, and the energetics of the problem is investigated. Finally, in § 6 the main conclusions are drawn.

2. Loop Model and Governing MHD Equations

The equilibrium magnetic field is straight, uniform, and pointing in the z -direction, $\mathbf{B} = B_0 \hat{\mathbf{e}}_z$. For applications to the solar corona, it is a good approximation to consider that the magnetic pressure dominates the gas pressure. This zero- β approximation allows us to choose an arbitrary density profile. As a model of a bundle of loops we use a superposition of N tiny, parallel cylinders with different radii and densities. In Cartesian coordinates, the cross-section of the density of each individual strand is assumed to have the following form,

$$\rho_i(x, y) = \rho_{0i} \exp \left[-\frac{(x - x_i)^2 + (y - y_i)^2}{a_i^2} \right], \quad (1)$$

where ρ_{0i} is the maximum density of the strand, x_i and y_i the position of the strand axis, and a_i the strand radius. The density of the multi-stranded model is defined as

$$\rho_0(x, y) = \sum_{i=1}^N \rho_i(x, y) + \rho_{\text{ex}}, \quad (2)$$

ρ_{ex} being the density of the external medium (assumed constant). Note that the density of a single uniform cylindrical loop, ρ_{in} , with radius R that has the same mass as the multi-stranded loop is simply,

$$\rho_{\text{in}} = \frac{1}{R^2} \sum_{i=1}^N \rho_{0i} a_i^2 + \rho_{\text{ex}}. \quad (3)$$

In Figure 1 the two-dimensional distribution of the density (the cross section of the composite loop) is plotted for a particular configuration based on equations (1) and (2). For this particular configuration the loop is composed of ten individual strands with their axis located at the following x_i and y_i coordinates: $[0, 0, -0.65, 0.65, 0.5, -0.5, -0.5, 0.5, 0.2, -0.2]$ and $[-0.45, 0.65, 0, 0, 0.5, 0.5, -0.5, -0.5, 0, -0.2]$. The radii of the strands (a_i/R) are $[0.2, 0.275, 0.25, 0.3, 0.2, 0.25, 0.2, 0.25, 0.25, 0.25]$, and the densities (ρ_{0i}/ρ_{00}) are $[0.8, 0.6, 0.4, 0.3, 0.5, 0.6, 0.4, 0.6, 0.4, 0.3]$. The external density is $\rho_{\text{ex}} = 1/3 \rho_{00}$, ρ_{00} being a reference density inside the loop.

We see that the loop density has an inhomogeneous distribution with quite an irregular cross section and irregular boundary. This model has a complex geometry compared with the usual cylindrical or the elliptical tubes usually used to study loop oscillations. In this so-called “spaghetti model” (see Bogdan & Fox 1991; Keppens et al. 1994) the distance between the strands is quite small and a strong dynamical interaction between them is expected. This kind of model has been previously considered in the context of scattering and absorption of sound waves in composite sunspot models.

To study small amplitude perturbations in this equilibrium we use the linearized ideal MHD equations. The equilibrium depends on x and y but it is independent of the longitudinal z -coordinate. For this reason, we Fourier analyze in this direction assuming a dependence of the form $e^{-ik_z z}$, k_z being the vertical wavenumber. We concentrate on the fundamental mode, with $k_z = \pi/L$, L being the length of the loop (here we use $L = 20R$). Under these assumptions the MHD equations are,

$$\rho_0 \frac{\partial v_x}{\partial t} + \frac{B_0}{\mu} \left(ik_z b_x + \frac{\partial b_z}{\partial x} \right) = 0, \quad (4)$$

$$\rho_0 \frac{\partial v_y}{\partial t} + \frac{B_0}{\mu} \left(ik_z b_y + \frac{\partial b_z}{\partial y} \right) = 0, \quad (5)$$

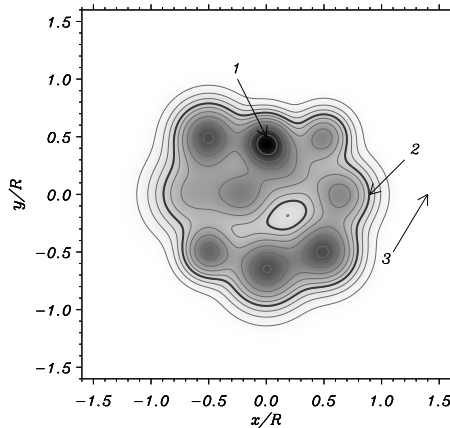


Fig. 1.— Cross section of the density of the multi-stranded loop model. The lengths are normalized to R , the reference radius of an individual homogeneous loop. The contour lines represent curves of constant Alfvén frequency, given by equation (10) (they also represent contours of constant density). The thick line corresponds to the Alfvén frequency that matches the frequency of the global mode. The labels 1, 2, and 3 indicate the locations analyzed in Figures 3, 4, and 5, respectively.

$$\frac{\partial b_x}{\partial t} + B_0 i k_z v_x = 0, \quad (6)$$

$$\frac{\partial b_y}{\partial t} + B_0 i k_z v_y = 0, \quad (7)$$

$$\frac{\partial b_z}{\partial t} + B_0 \left(\frac{\partial v_x}{\partial x} + \frac{\partial v_y}{\partial y} \right) = 0, \quad (8)$$

where $\mathbf{v} = (v_x, v_y, 0)$ is the velocity and $\mathbf{b} = (b_x, b_y, b_z)$ is the perturbed magnetic field. These equations can be rewritten as a system of five equations with five real variables using the transformations $b_x \rightarrow i b_x$ and $b_y \rightarrow i b_y$ (these variables are shifted $\pi/2$ in the z -direction with respect to v_x , v_y , and b_z). The equations are complemented with an initial perturbation located in the external medium. For simplicity we assume that it has the following form

$$v_y(x, y) = v_{y0} \exp \left[-\frac{(y - y_0)^2}{w^2} \right], \quad (9)$$

where v_{y0} is the amplitude of the perturbation (this parameter is arbitrary since we are in the linear regime), y_0 is the position of the center of the disturbance, and w is its width (here we use $y_0 = 3R$ and $w = R$, which means that the perturbation is located at a distance $3R$ from the center of the loop). All other MHD variables are initially set to zero. This perturbation is a planar pulse which produces the excitation of fast MHD waves that propagate and interact with the loop structure.

In the excitation of fast MHD waves and specially Alfvén waves an important quantity in our model is the local Alfvén frequency,

$$\omega_A(x, y) = k_z v_A(x, y) = k_z \frac{B_0}{\sqrt{\mu \rho_0(x, y)}}, \quad (10)$$

v_A being the Alfvén speed. The Alfvén frequency distribution in our equilibrium depends on x and y in a quite complicated manner, as we can see in Figure 1 (see the contours of constant ω_A represented with continuous lines). The fact that ω_A varies with position plays a key role for the resonant conversion of wave energy from global large scale motions to localized Alfvén modes.

3. Method

From the numerical point of view the problem that we are studying has basically two difficulties. The first one is related with the small spatial scales that are generated in the inhomogeneous layers, so we must make sure that we are properly resolving these layers. This point is crucial to have the correct energy conversion rates and in consequence the right damping times of transversal oscillations. Due to the phase mixing process (see Heyvaerts & Priest 1983), specially important at the inhomogeneous layers, the maximum time for which the simulations can be run is determined by the phase mixing length, defined as the length over which the phase of neighboring Alfvén waves differs by 2π (Mann et al. 1995; Wright & Rickard 1995),

$$L_{\text{ph}} = 2\pi / \left(t \frac{d\omega_A}{dx} \right). \quad (11)$$

Therefore, the typical spatial lengths decrease quickly with time. The shortest wavelength that can be resolved numerically with a uniform grid spacing of Δx is $\lambda = 2\Delta x$. We can run the simulations until the phase mixing length is equal to the shortest wavelength ($L_{\text{ph}} = \lambda$). Thus, the maximum simulation time is simply

$$t_{\text{max}} = \pi / \left(\Delta x \frac{d\omega_A}{dx} \right). \quad (12)$$

We have checked that this condition is not violated in the simulations (note that it also has to be satisfied in the y -coordinate).

The second difficulty is the effect of the boundaries on the loop dynamics. Even applying transparent boundary conditions (zero order extrapolation) at the limits of the computational domain, it is important to locate the boundaries far enough from the loop. Note that a

trapped mode in the loop has always an evanescent part in the external medium which might be affected by the conditions that we apply at the boundaries.

To solve these difficulties we have used a resolution sufficiently high to resolve the different scales (a grid of 4000×4000 points is sufficient) and to avoid significant reflections we have located the domain limits far enough from the loop, at $x_B = \pm 8R$, $y_B = \pm 8R$. Nevertheless, in order to better interpret and visualize the results the plots are displayed in a smaller spatial domain ($[-1.6R, 1.6R] \times [-1.6R, 1.6R]$).

To numerically solve the time-dependent MHD equations, equations (4)–(8), together with the initial condition, equation (9), we use the code CLAWPACK (Leveque 2004). This code implements a wide class of high-resolution finite volume methods for solving linear or nonlinear hyperbolic problems. Due to resolution requirements we have run the parallelized version of the code in a cluster of computers.

4. Test case: resonant absorption in an inhomogeneous cylindrical loop

Due to the different scales involved in the problem the modeling of resonant absorption is challenging from the numerical point of view. For this reason, before the “spaghetti model” is studied, it is necessary to check that the numerical method we are using is appropriate to study this problem. As a test we consider a single inhomogeneous cylindrical loop in two dimensions. To facilitate comparison of the time-dependent results with previous eigenmode studies we choose the same density profile as in Ruderman & Roberts (2002); Van Doorselaere et al. (2004a); Terradas et al. (2006a), i.e., a sinusoidal variation in density across the non-uniform layer. For such a configuration and for the $m = 1$ mode (the kink mode), the damping per period (the damping time, τ_d , over the period, P) in the limit of thin tube and thin boundary is

$$\frac{\tau_d}{P} = \frac{2 R \rho_{\text{in}} + \rho_{\text{ex}}}{\pi l \rho_{\text{in}} - \rho_e}, \quad (13)$$

where l is the thickness of the non-uniform layer and R is the loop radius. For thick layers the eigenvalue problem has to be solved numerically (see Van Doorselaere et al. 2004a; Terradas et al. 2006a). In our composed loop model there is a wide range of thicknesses, and for this reason we have calculated the eigenmodes of the cylindrical loop numerically (see Terradas et al. 2006a, for details about the method used to perform these calculations). In Figure 2 (top panel) the damping per period for a single cylindrical loop calculated from equation (13) and the eigenmode calculations are represented as a function of the thickness of the layer. The small differences between the two curves are simply due to the fact that equation (13) is inaccurate for thick layers (see also Van Doorselaere et al. 2004a).

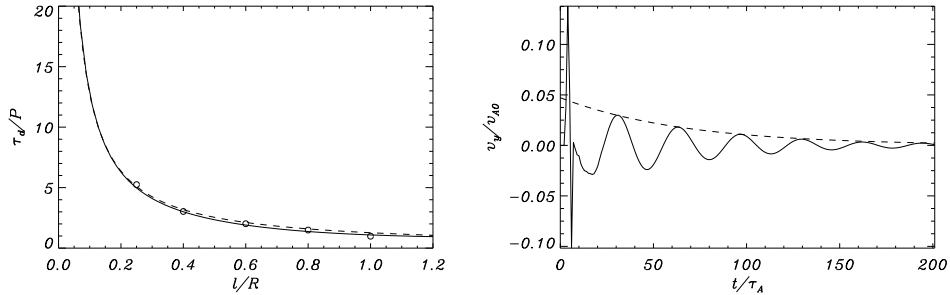


Fig. 2.— *Top panel:* Damping per period as a function of the thickness of the non-uniform layer for a single cylindrical loop ($\rho_{\text{ex}} = 1/3 \rho_{\text{in}}$, $k_z R = \pi/20$). The dashed line is the damping per period calculated using equation (13) while the continuous line is calculated with the eigenvalue problem for thick layers (see Terradas et al. 2006a). The circles represent the values calculated from the time-dependent two-dimensional simulations. *Bottom panel:* Plot of v_y at the center of the cylindrical loop as a function of time for the case $l/R = 0.6$. This result has been obtained by solving the time-dependent equations. The dashed line is a fit of the form $\exp(-t/\tau_d)$. The time is normalized to the Alfvén transit time, $\tau_A = v_{A0}/R$, where $v_{A0} = B_0/\sqrt{\mu\rho_{\text{in}}}$.

To compare the results of these eigenmode calculations with the time-dependent problem we need to place an initial perturbation in the system that basically excites the kink mode (the eigenmode calculations that we want to compare with are for this mode, $m = 1$). The planar pulse perturbation given by equation (9) is the kind of disturbance with such a property because an external perturbation hardly excites high order harmonics such as the fluting modes, and the sausage modes are leaky in our configuration (see Terradas et al. 2007b). We have run the code with this perturbation and have studied the subsequent evolution. Figure 2 (bottom panel) shows the plot of v_y at the center of the loop as a function of time for a particular thickness of the layer (see Fig. 4 in Terradas et al. 2006a, for the analogous simulation in 1D). After a short transient the loop oscillates with the quasi-mode period and the amplitude of the mode is attenuated due to the energy conversion in the inhomogeneous layer. From the results of the simulations we calculate the period, P , by performing a periodogram. The damping time, τ_d , is numerically estimated by fitting an exponential function of the form $\exp(-t/\tau_d)$ to the envelope of the curve. We have performed several simulations varying the width of the layer and the numerically obtained damping per periods are represented with circles in Figure 2 (top panel) as a function of the thickness of the layer. We find the expected dependence with l/R and we see that the deviations from the eigenmode calculations are quite small. It is important to remark that, although we model a cylindrical tube, in these simulations we use Cartesian coordinates and we still obtain the right damping rates.

In conclusion, with this simple numerical experiment we demonstrate that we are using a reliable tool to study resonant absorption. Note that contrary to some precedent works, where a large amount of resistivity is used mainly to avoid numerical problems, here we are in ideal MHD conditions. Hence, the system dynamics is not dominated by the resistive regime, in this case the behavior in Figure 2 (top panel) would be completely different, the damping time being independent of l/R (see for example Fig. 2 in Terradas et al. 2006a).

5. Results: multi-stranded model

We now use the multi-stranded model shown in Figure 1 and study how the system evolves due to a planar pulse perturbation (eq. [9]). The initial pulse produces a displacement of the whole ensemble of strands basically in the y -direction, i.e. the direction in which the initial perturbation propagates. The initial stage of the evolution of the bundle of loops is dominated by a complicated set of internal reflections of the wavefront between the different strands. During this transient several wavefronts propagating from the bundles into the external medium are found. They correspond to the emission of the leaky modes representing fast radiating MHD waves with short periods and fast attenuation (see Cally 1986, 2003; Terradas et al. 2007a, for the analysis of such modes in a single cylindrical loop). After the transient the system periodically oscillates with certain frequencies. Hereafter, we concentrate on this stage of the dynamics.

5.1. Frequency analysis

We first investigate the characteristic frequencies of the system. An analysis of the results of the simulations shows that inside the loop there are basically two dominant frequencies at each point. One is the collective frequency of the bundle of loops (different from the kink frequency of the individual strands) and the other is the local Alfvén frequency, ω_A . The collective frequency is the result of the excitation of the global mode of the system which represents the emergent behavior of the entire loop. On the other hand, the local Alfvén frequency is due to the excitation of the Alfvén continuum modes. As an example, in Figure 3 the v_y velocity component as a function of time (top panel) and its power spectrum (bottom panel) are represented at an interior point (see label 1 in Fig. 1). The two dominant frequencies, the local Alfvén frequency and the global frequency (with the largest power) are clearly identified in the power spectrum. Note the strong decrease of the amplitude with time. This attenuation is found almost everywhere at the interior points and suggests a collective motion of the bundle of tubes. We have also represented in Figure 3 (top panel)

the other component of the velocity, v_x . Its amplitude is smaller than the v_y component and it does not show attenuation with time.

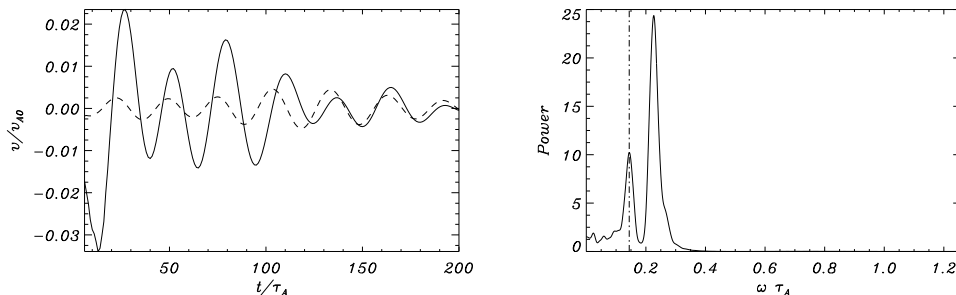


Fig. 3.— *Top panel:* Time evolution of the v_x (dashed line) and v_y (continuous line) velocity components at the interior point $x = 0$, $y = 0.5R$ (see label 1 in Fig.1). *Bottom panel:* Power spectrum of the v_y velocity component. The peak with the largest power corresponds to the global mode while the weaker peak is due to the excitation of the local Alfvén mode. The local Alfvén frequency, calculated from the function $\omega_A(x, y)$, at the coordinates of the previous point is represented with dot-dashed lines and agrees with the location of the weak peak.

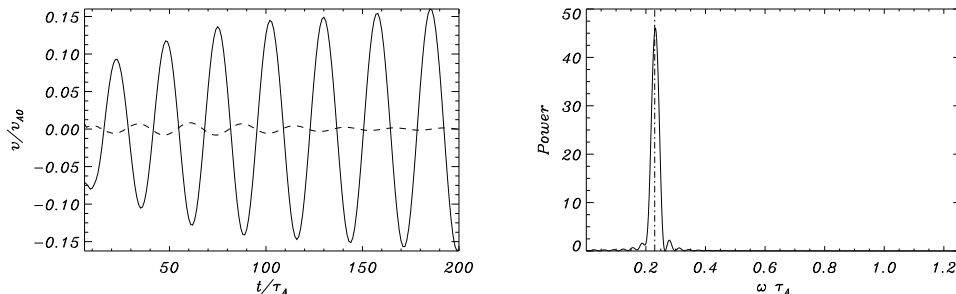


Fig. 4.— *Top panel:* Time evolution of the v_x (dashed line) and v_y (continuous line) component at a position near the loop edge, $x = 0.9R$, $y = 0$ (see label 2 in Fig.1). *Bottom panel:* Power spectrum of the v_y velocity component. The local Alfvén frequency is represented with dot-dashed lines.

There are particular locations in the structure where the behavior of the signal is completely different. An example is shown in Figure 4 which corresponds to a position situated near the loop edge (see label 2 in Fig. 1). Now, instead of a damped oscillation, the amplitude of the v_y velocity component grows with time while the v_x component decreases. There is just a single peak in the power spectrum because the local and the global frequencies coincide. As we will show in the following sections this is the place where the energy conversion takes place.

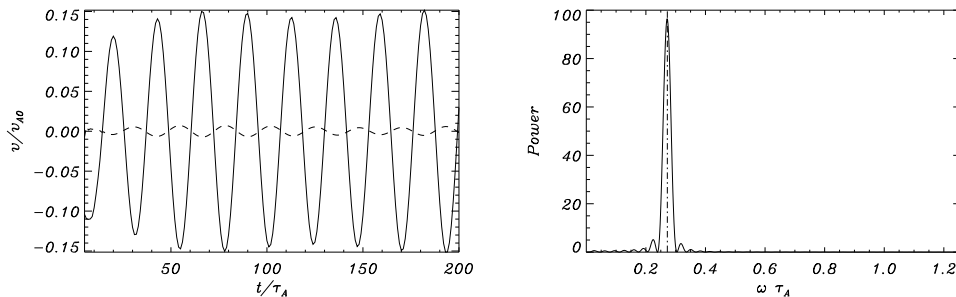


Fig. 5.— *Top panel:* Time evolution of the v_x (dashed line) and v_y (continuous line) component at a position near the loop edge, $x = 1.4R$, $y = 0$ (see label 3 in Fig.1). *Bottom panel:* Power spectrum of the v_y velocity component. The local Alfvén frequency, i.e. for this particular point the external Alfvén frequency, is represented with dot-dashed lines.

Outside the structure, oscillations tending to the Alfvén frequency are found everywhere, see for example the velocity represented in Figure 5 (see label 3 in Fig. 1). These oscillations are basically produced by the wake of the initial fast MHD perturbation and have a large amplitude compared with the amplitude inside the loop (see Fig. 3). This wake oscillates (in the limit of large times) at the local Alfvén frequency (see Terradas et al. 2005) which is precisely where the dominant peak is found in the power spectrum. However, it is worth noticing that near the loop edge, but in the external medium, the quasi-mode frequency is also present. This is not surprising, since the quasi-mode has an evanescent tail in the external medium.

We have also performed the same analysis but for the b_z component, which is proportional to the total pressure perturbation ($P_T = b_z B_0/\mu$). We have found large power at the global mode frequency and very weak power around the local Alfvén frequency. This is because pure Alfvén modes do not perturb the total pressure and, although in our configuration Alfvén modes are coupled with fast modes, they still keep a strong incompressible character.

5.2. Velocity field

To explain the different behavior of the velocity at different locations in the structure we need to understand the evolution of the whole system instead of looking at individual points. In Figure 6 the velocity components v_x , v_y are plotted at $t = 40 \tau_A$. Inside the loop the v_x component is quite uniformly distributed while the v_y component has a complicated spatial structure which basically coincides with the spatial distribution of the strands (see

the contours). At this particular instant the higher the density of the strand the smaller the amplitude of the v_y component. On the other hand, the velocity components outside the loop have quite a smooth spatial distribution. The motion of the whole structure is clearer if we represent the velocity field constructed using the v_x and v_y components. The result is shown in the top panel of Figure 7. We clearly see that all the strands are moving in the negative y -direction and that the external medium reacts in a very organized way to the displacement of the bundle of loops. The plasma at the bottom of the loop ($y \approx -R$) is pushed sideways while the plasma at the top of the structure ($y \approx 0.8R$) tends to fill the region that has displaced downwards. This motion is the equivalent of the kink mode in a cylindrical tube.

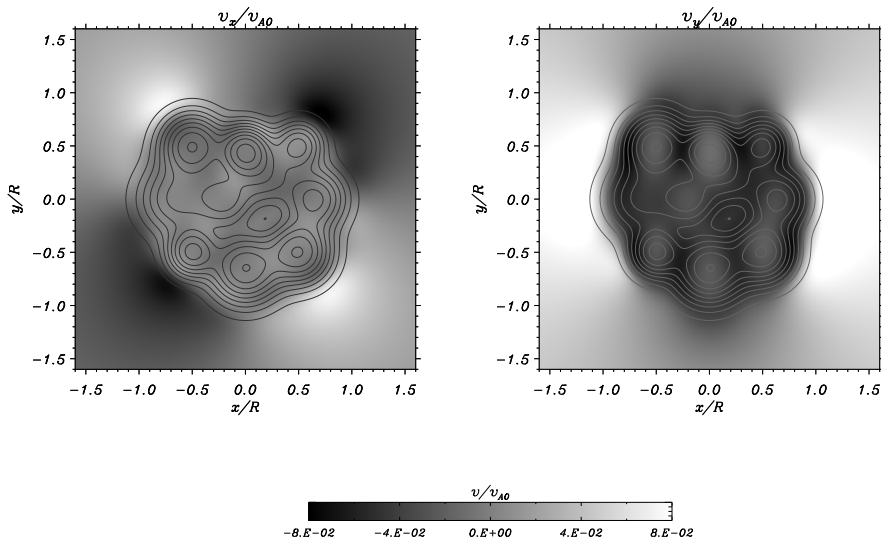


Fig. 6.— Spatial distribution of the v_x velocity component (*top panel*), v_y velocity component (*bottom panel*) at $t = 40 \tau_A$. The corresponding velocity field is plotted in the top panel of Figure 7. Contours of constant Alfvén frequency are represented with continuous lines.

At later times (see the middle and the bottom panels in Fig. 7) large amplitude velocities develop specially near the external edge of the composite loop. This is the consequence of the energy conversion between the global mode and the Alfvén modes. Due to this process the global oscillation gradually loses its energy and its amplitude is attenuated in time (see for example the length of the arrows at the centers of the individual strands in Fig. 7 at $t = 160 \tau_A$). This explains the attenuation of v_y found in Figure 3. On the other hand, the amplitude of the Alfvén modes increases at the resonant layers where the energy conversion takes place (see the large arrows at the loop boundaries in Fig. 7, bottom panel). We already found this behavior in Figure 4.

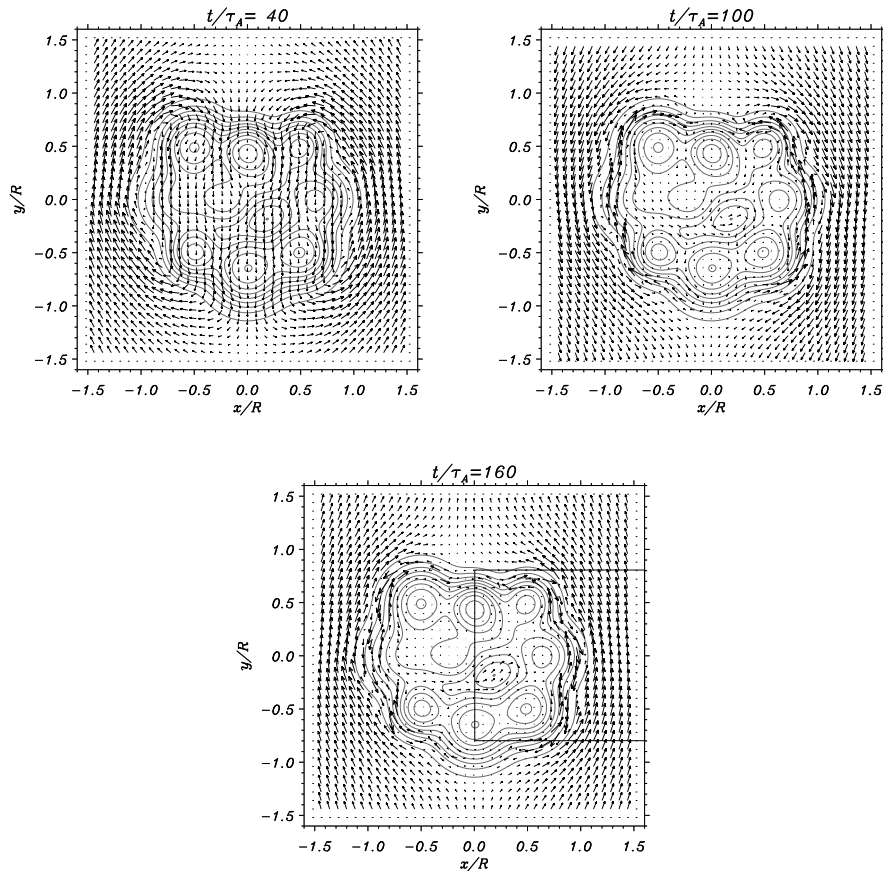


Fig. 7.— Time evolution of the velocity field. The loop initially oscillates in the y direction with the global mode. Due to the mode conversion motions localized on the magnetic surfaces develop (see the contours of constant Alfvén frequency represented with continuous lines). The region marked with a square box in the bottom panel is plotted in Figure 8. This figure is also available as an mpeg animation in the electronic edition of the *Astrophysical Journal*.

Since the Alfvén frequency changes with position the Alfvénic motions get out of phase very quickly due to phase mixing. The consequence of this process is visible at the external boundaries where strong shear motions develop. To see these motions in detail we have concentrated on the small region marked with a square box in Figure 7 bottom panel. The result is plotted in Figure 8. We see that the field is organized and that near the edge of the loop the velocity vectors are aligned with the contours of constant Alfvén frequency (see the continuous lines). It is also clear that on neighboring magnetic surfaces motions are basically in opposite directions. This is even clearer in Figure 9 where we have plotted a cut of v_y at $y = 0$ (see the continuous line). This figure also shows how this component of the velocity field (which is mainly parallel to the magnetic surfaces around $x = R$) evolves

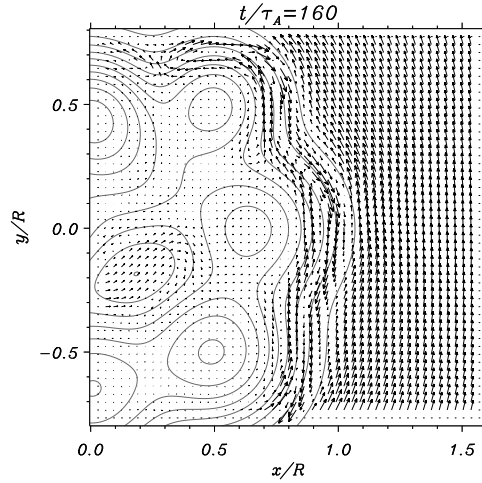


Fig. 8.— Detail of the velocity field at $t = 160 \tau_A$, see square box in the bottom panel of Figure 7.

with time. As expected from the phase mixing process, the typical spatial scales of the shear motions decrease with time. The amplitude of the velocity decreases in the internal part of the structure while it develops short wavelengths around the resonant positions. We find that the typical wavelengths agree with the phase mixing lengths, L_{ph} , predicted by equation (11) (compare the lengths of the lines in the legend of the plot with the wavelengths of v_y at $x = R$).

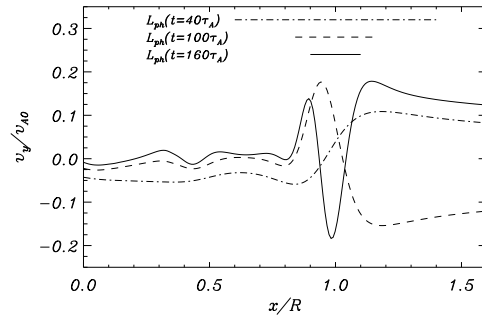


Fig. 9.— Plot of v_y as a function of x ($y = 0$) at $t = 40 \tau_A$ (dot-dashed line), $t = 100 \tau_A$ (dashed line), and $t = 160 \tau_A$ (continuous line). The lengths of the lines plotted in the legend correspond to the phase mixing lengths, L_{ph} , predicted by equation (11) at the position $x = R$ ($y = 0$).

At this point it is worth noticing that due to mode coupling Alfvén modes are excited everywhere in the structure even at locations far from the resonance. The excitation of these modes is already known, specially in driven problems (see for example Mann et al.

1995; Tirry et al. 1997; Goossens & De Groof 2001), but there are still several questions about these modes that need to be addressed, as for example the amount of energy that is deposited in the Alfvén modes. In any case, far from the resonance, the amplitude of these modes is smaller than the amplitude of the global mode (on average). We see in Figure 3 (bottom panel) that for this internal position the amplitude of the global oscillation, in the v_y component, is around 1.5 times the amplitude of the Alfvén modes (the power of the peaks, proportional to the square of the amplitude, are around 24 and 10). A more detailed analysis, out of the scope of this work, is required.

5.3. Energy distribution

The process of mode conversion is even clearer if we study the energetics of the system. For this reason we now focus on the wave energy density. Since in our model we adopt the zero- β approximation there are only contributions from the kinetic and magnetic energy to the total wave energy,

$$E = \frac{1}{2} \left[\rho_0 (v_x^2 + v_y^2) + \frac{1}{\mu} (b_x^2 + b_y^2 + b_z^2) \right]. \quad (14)$$

This quantity is represented in Figure 10 at different times (same as in Fig. 7). The plots show that the system evolves from a situation where the energy is more or less uniformly distributed to a state in which it is concentrated around the resonant layers. The wave energy is spatially distributed in such a way that it follows the irregular geometry of the loop edge (see the bright areas on the left and right loop boundaries). Out of the resonances the energy decreases with time, see the interior points, except for the area around $x = 0.2R$, $y = -0.2R$ where we can find some energy for large times. It should be also noted that the system evolves so that the resonance energy width decreases with time. This behavior of the wave energy at the resonance has been described in detail by Mann et al. (1995) (see also the equivalent results in a cylindrical inhomogeneous loop, Fig. 8, in Terradas et al. 2006a). To see these effects more clearly we have concentrated on a slice at $y = 0$ (see Fig. 11) and have plotted the wave energy density at different times. This figure shows that the energy width decreases with time at the external boundaries, basically at $x = R$ and $x = -R$. We also see the peak around $x = 0.3R$, and the energy decrease with time in the range $-0.8 < x/R < 0.1$ and $0.5 < x/R < 0.7$.

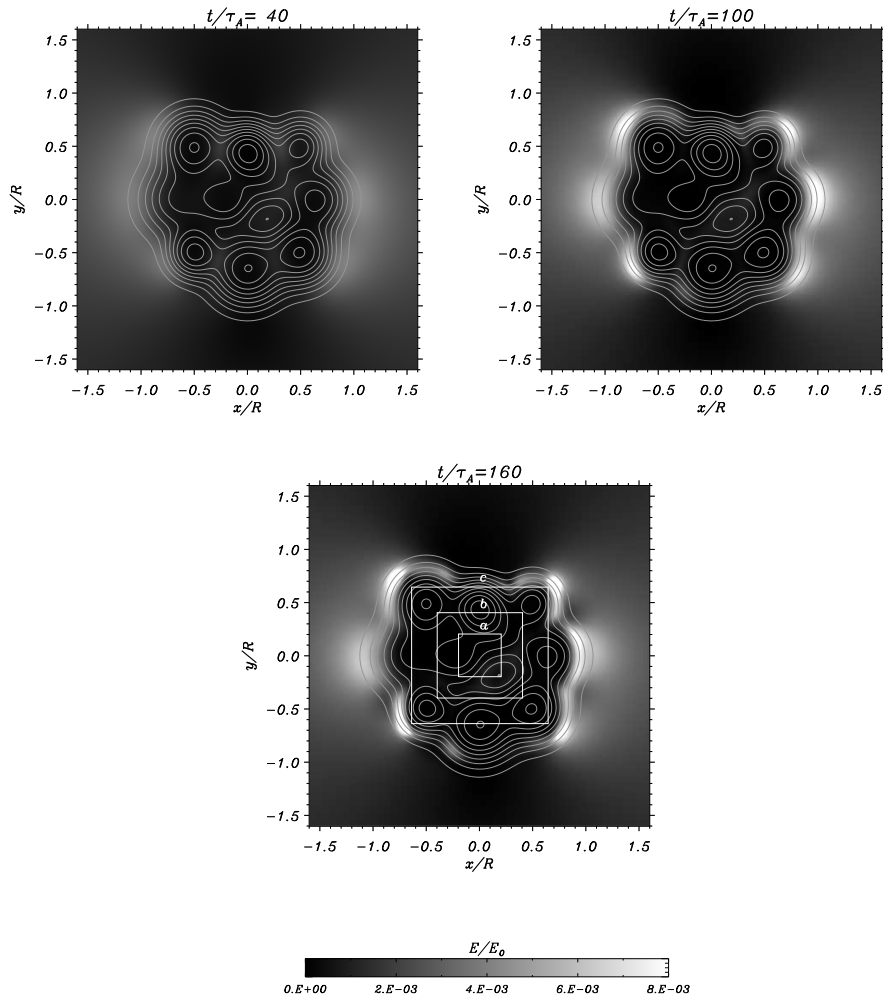


Fig. 10.— Time evolution of the energy distribution for the same simulation as in Figure 7. The three square boxes labeled with a , b , and c in the bottom panel mark the regions where the velocity averages have been computed to determine the damping time (see Fig. 12). This figure is also available as an mpeg animation in the electronic edition of the *Astrophysical Journal*.

5.4. Resonant magnetic surfaces

It is quite evident from the velocity and energy analysis where the energy conversion takes place. However, we can be more precise in the determination of the resonant magnetic surface or surfaces. Once we know the frequency of the global mode the location of the resonances is basically where this frequency coincides with the local Alfvén frequency. In Figure 1 contours of the Alfvén frequency, ω_A , are represented together with the global frequency, see the contours with thick lines. In this plot we find that there are two resonant

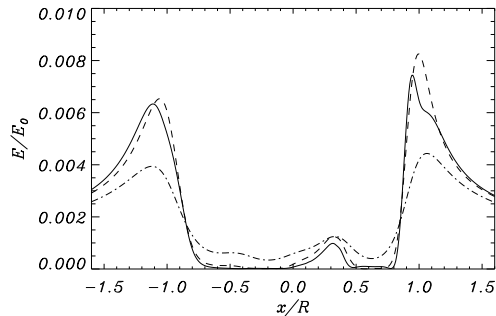


Fig. 11.— Wave energy density, calculated using equation (14), as a function of x ($y = 0$) for three different times (same as in Fig. 10, the same notation as in Fig. 9 has been used for the lines). The energy concentrates around the external edges of the loop (some part also concentrates inside the structure, around $x = 0.3R$). The width of the energy peaks around the resonant layers decreases with time. Note also the decrease of energy in the internal part of the loop.

magnetic surfaces. One surface is located at the external edge of the composite loop and the other resonant magnetic surface is located inside the structure (see the small hole around $x = 0.2R$, $y = -0.2R$). It is precisely at these locations where the energy maps show enhanced energy, see for example Figure 10 bottom panel, and also where the highest velocity amplitudes are found, see Figure 7. Thus, for this particular multi-stranded configuration, resonant absorption not only takes place at the external boundaries, but some energy is also deposited in the internal part of the composite structure.

5.5. Damping time

Due to the simultaneous excitation of the quasi-mode and the local Alfvén modes, the determination of the damping rates of the loop oscillation can be quite difficult (see for example the time series in Fig. 3). However, there is a simple way to estimate the damping time. We have taken uniformly distributed regions inside the loop and have added up the velocity field at a given instant. This basically averages out the contribution of the local Alfvén modes since these modes develop small spatial scales. At the same time the average enhances the coherent behavior of the global mode, having a large spatial length. In Figure 12 we have represented the averaged signal as a function of time for three regions inside the loop (see the boxes labeled with letters a , b , and c in Figure 10 bottom panel). We see that we get almost the same time dependence for the different regions in the loop, indicating that the global mode is dominant everywhere inside the loop. Although the structure is quite inhomogeneous and irregular the damping time is basically the same everywhere. Now from

the averaged signal we can calculate the damping time using the same method as in the comparison with the cylindrical tube, i.e. by fitting an exponentially decaying function. We finally find that the damping per period is $\tau_d/P = 2.3$.

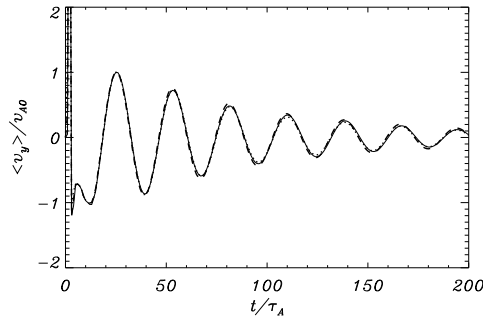


Fig. 12.— Time evolution of the spatially averaged v_y component as a function of time. The continuous, dot-dashed, and dotted lines correspond to the (normalized) averages in the square regions marked with labels a , b , and c in Figure 10 (bottom panel), respectively. The profile of the three signals is almost the same since the loop is oscillating with the global mode. The damping per period is $\tau_d/P = 2.3$.

6. Discussion and Conclusions

We have studied the mechanism of resonant absorption by solving the time-dependent problem of the excitation of oscillations in a complicated multi-stranded coronal loop. We have shown that the mode conversion takes place in quite irregular geometries like the one studied in this paper and that regular magnetic surfaces (considered in previous works) are not necessary for this mechanism to work efficiently. This suggests that resonant absorption is quite a robust damping mechanism. Although we have analyzed a particular system, the behavior found in the present equilibrium is expected to be quite generic of inhomogeneous plasma configurations. Since inhomogeneity is certainly present in coronal loops, the resonant coupling between fast and Alfvén modes can hardly be avoided in a real situation. For this reason, resonant absorption seems to be quite a natural damping mechanism.

The fact that the loop is not monolithic does not affect much the global oscillatory properties. Although the loop is composed of different strands we find a dominant frequency almost everywhere in the structure, indicating a global motion. It is interesting to compare the frequency of this global mode or quasi-mode with the frequency of the equivalent homogeneous loop with radius R and the same mass. Using equation (3) we find that the equivalent cylindrical loop should have an internal density $\rho_{\text{in}} = 0.67\rho_{00}$. The kink mode

period for a cylindrical tube with this internal density is $P = 28.4 \tau_A$. This value is in good agreement with the period of the quasi-mode estimated from the numerical simulations of the multi-stranded model, which is around $P = 28.0 \tau_A$. This indicates that the internal structure does not change much the global behavior of the loop (see also Arregui et al. 2007). Nevertheless, it may have some effect on the location of the energy deposition. We have found that in our model there is also energy conversion inside the loop, although it is small compared with the energy at resonances in the external layers.

Although at any time and at any position both the quasi-mode and the local Alfvén modes are excited, we have been able to estimate the damping time of the quasi-mode by performing averages of the dominant velocity component in different regions of the loop. The average eliminates the local Alfvén modes and enhances the global mode and is basically what the observations provide, a sort of integration along the line of sight (but in the displacement instead of the velocity).

On the other hand, it must be noted that a system of N tubes, like the one studied in this paper, is expected to have a large number of eigenmodes. For example, in a configuration with just two loops Luna et al. (2007) have shown that there are four kink-like eigenmodes, and that an external disturbance in general excites these four modes. However, these authors have shown that since their frequencies are very similar it is very difficult to distinguish between the different eigenmodes in a time-dependent study. For this reason, the interpretation of the global mode found in our multi-stranded loop as a sum of different eigenmodes with similar frequencies and similar damping times needs to be considered. This could explain the small differences in the period and damping time of the velocity averages in different regions of the structure. A detailed analysis of this issue is out of the scope of this paper but it is clear that the calculation of the eigenmodes of complicated configurations is very important. In this regard, analytical studies based on scattering theory will allow us to calculate the eigenmodes of a system of N tubes (Luna et al. 2008, in preparation) and to make progress in this direction.

Finally, it must be noted that we have concentrated on the linear regime. If the amplitude of the oscillations becomes large in the inhomogeneous layer due to mode conversion, non-linear terms might be important and the efficiency of resonant absorption can be altered. However, diffusion or viscosity may prevent the development of large amplitudes around the resonant layer. In addition, there are some results that indicate that in the non-linear regime the heating at the resonant layers may produce significant changes in the equilibrium configuration (see Ofman et al. 1998; Klimchuk 2006). Hence, the initial value problem needs to be studied using the full non-linear equations, which basically means that, since the Fourier analysis is no longer possible in the z -direction, the problem is three-dimensional. Due

to the grid resolution requirements in the layers the three-dimensional problem has a high computational cost. The numerical study presented here for the two-dimensional problem is a preliminary step to investigate resonant absorption in more realistic three-dimensional models including, for example, twisted or tangled magnetic fields.

J. Terradas is grateful to the Spanish Ministry of Education and Science for the funding provided under the Juan de la Cierva program. Funding provided under grants AYA2006-07637, of the Spanish Ministry of Education and Science, and PRIB-2004-10145 and PCTIB-2005GC3-03, of the Conselleria d'Economia, Hisenda i Innovació of the Government of the Balearic Islands, is also acknowledged.

REFERENCES

- Andries, J., Tirry, W. J., & Goossens, M. 2000, *ApJ*, 531, 561
- Andries, J., & Goossens, M. 2000, *A&A*, 368, 1083
- Andries, J., Goossens, M., Hollweg, J. V., Arregui, I., & Van Doorselaere, T. 2005, *A&A*, 430, 1109
- Arregui, I., Van Doorselaere, T., Andries, J., Goossens, M., & Kimpe, D. 2005, *A&A*, 441, 361
- Arregui, I., Terradas, J., Oliver, R., & Ballester, J. L. 2007, *A&A*, 466, 1145
- Aschwanden, M. J. 2005, *ApJ*, 634, L193
- Aschwanden, M. J., & Nightingale, R. W. 2005, *ApJ*, 633, 499
- Bogdan, T. J., & Fox, D. C. 1991, *ApJ*, 379, 758
- Cally, P. S. 1986, *Sol. Phys.*, 103, 277
- Cally, P. S. 2003, *Sol. Phys.*, 217, 95
- Davila, J. M 1987, *ApJ*, 317, 514,
- De Groof, A., Goossens, M. 2000, *A&A*, 356, 724
- De Groof, A., Goossens, M. 2002, *A&A*, 386, 691
- Erdélyi, R., & Goossens, M. 1996, *A&A*, 313, 664

- Goossens, M., Hollweg, J. V., & Sakurai, T. 1992, *A&A*, 138, 233
- Goossens, M., Ruderman, M. S., & Hollweg, J. V. 1995, *Sol. Phys.*, 157, 75
- Goossens, M., & De Groof, A. 2001, *Phys. Plasma*, 8, 2371
- Goossens, M., Andries, J., & Aschwanden, M. J. 2002, *A&A*, 394, L39
- Grossmann, W., & Smith, R. A. 1988, *ApJ*, 332, 476
- Heyvaerts, J., & Priest, E. R. 1983, *A&A*, 117, 220
- Hollweg, J. V. 1987, *ApJ*, 312, 880
- Hollweg, J. V., & Yang, G. 1988, *J. Geophys. Res.*, 93, A6, 5423
- Hollweg, J. V., Yang, G., Cadez, V. M.; Gakovic, B. 1990, *ApJ*, 349, 335
- Ionson, J. A. 1978, *ApJ*, 226, 650
- Keppens, R., Bogdan, T. J., & Goossens, M. 1994, *ApJ*, 436, 372
- Klimchuck, J. A. 2006, *Sol. Phys.*, 234, 41
- Lee, M. A., & Roberts, B. 1986, *ApJ*, 301, 430
- Leveque, R., *Finite Volume Methods for Hyperbolic Problems*, Cambridge University Press, Cambridge, 2002
- Luna, M, Terradas, J., Oliver, R., & Ballester J. L. 2007, *ApJ*, in press
- Luna, M, Terradas, J., Oliver, R., & Ballester J. L. 2008, in preparation
- Mann, I. R., Wright, A. N., & Cally, P. S. 1995, *J. Geophys. Res.*, 100, A10, 19441
- Martens, P. C. H., Cirtain, J. W., & Schmelz, J. T. 2002, *ApJ*, 577, L115
- Ofman, L., Davila, J. M., & Steinolfson, R. S. 1994, *ApJ*, 421, 360
- Ofman, L., Davila, J. M. 1995, *Jour. Geophys. Research*, 100, A12, 23,427
- Ofman, L., Davila, J. M., & Steinolfson, R. S. 1995, *A&A*, 441, 471
- Ofman, L., Klimchuk, J. A., & Davila, J. M. 1998, *ApJ*, 493, 474
- Poedts, S., Goossens, M., & Kerner, W. 1989, *Sol. Phys.*, 123, 83

- Poedts, S., Goossens, M., & Kerner, W. 1990, *ApJ*, 360, 279
- Poedts, S., & Kerner, W. 1991, *PRL*, 66, 22
- Ruderman, M. S. 2003, *A&A*, 409, 287
- Ruderman, M. S., & Roberts, B. 2002, *ApJ*, 577, 129
- Sakurai, T., Goossens, M., & Hollweg, J. V. 1991, *Sol. Phys.*, 133, 227
- Schmelz, J. T., Nasraoui, K., Richardson, V. L. et al. 2005, *ApJ*, 627, L81
- Steinolfson, R. S., & Davila, J. M. 1993, *ApJ*, 415, 354
- Terradas, J., Oliver, R., & Ballester J. L. 2005a, *ApJ*, 618, L149
- Terradas, J., Oliver, R., & Ballester J. L. 2006a, *ApJ*, 642, 533
- Terradas, J., Oliver, R., & Ballester J. L. 2006b, *ApJ*, 650, L91
- Terradas, J., Andries, J., & Goossens, M. 2007, *Sol. Phys.*, 246, 231
- Terradas, J., Andries, J., & Goossens, M. 2007, *A&A*, 469, 1135
- Tirry, W. J., & Goossens, M. 1996, *ApJ*, 471, 501
- Tirry, W. J., Berghmans, D., & Goossens, M. 1997, *A&A*, 322, 329
- Tirry, W. J., Cadez, V. M., Erdéyi, R., & Goossens, M. 1998, *A&A*, 322, 786
- Van Doorselaere, Andries, J., Poedts, S., & Goossens, M. 2004, *ApJ*, 606, 1223
- Van Doorselaere, T., Debosscher, A., Andries, J., & Poedts, S. 2004, *A&A*, 424, 1065
- Wright, A. N., & Rickard, G. J. 1995, *ApJ*, 44, 458